Angular dependence of the H-T phase diagram of $CsNiCl_3$

Y. Trudeau, M. L. Plumer, M. Poirier, and A. Caillé
Centre de Recherche en Physique du Solide, Département de Physique, Université de Sherbrooke, Sherbrooke, Québec, Canada J1K 2R1
(Received 15 June 1993)

The results of an ultrasonic study of the magnetic-field–temperature (H-T) phase diagram of hexagonal $CsNiCl_3$ as a function of the angle between the magnetic field and the $\hat{\mathbf{c}}$ axis are presented. Upon rotation of the field, the structure of the phase diagram is modified from four phases joined at a multicritical point for $\mathbf{H} \parallel \hat{\mathbf{c}}$ to three phases without a multicritical point at other field directions. A previously unseen transition has been detected at intermediate field angles. The behavior of the spin-flop anomaly on the acoustic velocity is also investigated as a function of field angle and temperature. The amplitude of this anomaly has been found to exhibit a strong dependence on these two parameters. An analysis of these phase diagrams has been made using a nonlocal Landau free-energy approach [Phys. Rev. Lett. **60**, 45 (1988)].

I. INTRODUCTION

The last decade has seen a continuing interest in the magnetic properties of the hexagonal insulators belonging to the ABX_3 family, where B represents a magnetic ion such as Ni, Mn, and Co. In these systems, the magnetic ions are grouped in $\hat{\mathbf{c}}$-axis chains that are relatively well isolated from each other. This structural anisotropy causes the magnetic properties to have a strong quasi-one-dimensional behavior. The Hamiltonian describing such systems is

$$H = -2J_{\parallel} \sum_i \mathbf{S}_i \cdot \mathbf{S}_{i+1} - J_{\perp} \sum_{i \neq j} \mathbf{S}_i \cdot \mathbf{S}_j - D \sum_i (S_i^z)^2 - \mathbf{H} \cdot \sum_i \mathbf{S}_i \ , \quad (1)$$

where $J_{\parallel}$ and $J_{\perp}$ are the antiferromagnetic intra- and interchain nearest-neighbor exchange interactions, respectively, and $D > 0$ is the single-ion axial anisotropy. A quasi-one-dimensional system is defined by $J_{\parallel}/J_{\perp} \gg 1$.

Many studies, both theoretical and experimental, have been conducted on these systems and they can be separated roughly into two groups; the ones interested in the spin-wave properties and the ones interested in the low-temperature phase diagrams. On one hand, the Haldane conjecture[1] has received a lot of attention recently in connection with the spin-wave properties and many ABX_3 ($S = 1$) systems like $CsNiCl_3$ and $RbNiCl_3$ are now considered to be good candidates. On the other hand, the presence of competing interactions and also frustration resulting from the triangular structure can yield complex phase diagrams at low-temperature (in addition to modifying the spin-wave structure[2]). This is especially true for systems like $CsNiCl_3$, $CsNiBr_3$, and $CsMnI_3$ where multicritical points can be observed. The present investigation belongs to the second group and it concerns a well-known easy-axis quasi-one-dimensional antiferromagnet crystal, $CsNiCl_3$. This compound is known to be very stable and much less hydroscopic than other crystals of the same family like $CsMnI_3$, two desirable qualities for experimental work.

The parameters of the Hamiltonian (1) for $CsNiCl_3$, reported by Buyers *et al.*,[3] are $J_{\parallel}/k = -16.6$ K, $J_{\perp}/k = -0.29$ K, and $D/k = 0.63$ K. From previous experimental and theoretical work, in zero magnetic field we can expect[4–7] to have at least three phases: a paramagnetic (P) at high temperature, a linear (L) state at intermediate temperature, and an elliptical 120° (E) phase at low temperature when the thermal fluctuations are too small to screen $J_{\perp}$. In the presence of a magnetic field parallel to the chains axis ($\hat{\mathbf{c}}$ axis) there is also a spin-flop (SF) phase when the field is large enough to overcome the single-ion anisotropy. There is no such transition when $\mathbf{H} \perp \hat{\mathbf{c}}$ since in this configuration the field and the single-ion anisotropy are not in competition. In the literature,[7] these phases are respectively labeled 1, 2, 3, and 4. When the magnetic field is neither along the $\hat{\mathbf{c}}$ axis, nor in the plane, the phases 2 and 3 have slightly different symmetries and they are labeled 9 and 8, respectively, as discussed in Sec. IV.

The phase diagrams with $\mathbf{H} \parallel \hat{\mathbf{c}}$ and $\mathbf{H} \perp \hat{\mathbf{c}}$ are well known and they differ considerably. They were obtained from susceptibility,[5] neutron-scattering,[3] and ultrasonic[6] data. The purpose of the present work is to investigate the evolution of the phase diagram between these two extremes. We report here, in addition to results for $\mathbf{H} \parallel \hat{\mathbf{c}}$ and $\mathbf{H} \perp \hat{\mathbf{c}}$, the phase diagrams with $\mathbf{H}$ directed 5, 10, 20, 30, and 50° away from $\hat{\mathbf{c}}$. It is our experience[6,8] that ultrasound is a very effective and economical way to probe the magnetic properties of $CsNiCl_3$, especially in the region close to the multicritical point. So, the transition lines reported here, were obtained with an ultrasonic technique in temperature and magnetic field ranges of 2–6 K and 0–6 T, respectively. We have also extracted from the raw data of the acoustic velocity some interesting behavior of the anomaly at the E-SF transition as a func-

0163-1829/93/48(17)/12805(8)/$06.00

tion of field direction and temperature. These results are analyzed using the phenomenological Landau-type free energy model developed by Plumer, Hood, and Caillé.[7] This work serves to compliment and extend an earlier ultrasonic investigation[6] of the phase diagram where results were reported only for $\mathbf{H} \parallel \hat{\mathbf{c}}$.

II. EXPERIMENT

The acoustic velocity was measured with a pulsed acoustic interferometer whose operating principle is based on the measurement of the phase difference between the acoustic wave and a reference signal.[9] This phase difference is inversely proportional to the acoustic velocity v according to the relation

$$\phi = \frac{2\pi f n L}{v}, \tag{2}$$

where n, L, and f are, respectively, the number of back-and-forth trips executed by the acoustic pulse, the length of the sample, and the rf frequency. During the experiment, when the external parameters (H,T) are modified, the phase difference is maintained constant by a frequency feedback loop. The relative velocity variation is then given by

$$\frac{\Delta v}{v} = \frac{\Delta f}{f} + \frac{\Delta L}{L}. \tag{3}$$

Since the thermal expansion[10] and the magnetostriction[11] are orders of magnitude smaller than the variation of velocity due to either the magnetic field or the temperature for the ranges used, they are neglected. The attenuation is obtained from the amplitude of the first acoustic transmitted pulse at the output of the sample. Particular care has been taken to account for the nonparallelism and the finite bandwidth of the transducers.

The single crystal used for this experiment was grown by the Bridgman method. Its tendency to cleave along the 1120 plane facilitated its orientation for acoustic propagation along the $\hat{\mathbf{c}}$ axis [0001]. Parallel faces, approximately 10 mm apart with normals parallel to the $\hat{\mathbf{c}}$ axis, were polished to receive the acoustic transducers. In this work we have used Y-cut coaxially plated $LiNbO_3$ piezoelectric transducers, having a fundamental frequency of 30 MHz to produce the longitudinal acoustic pulses. Precision better than 1 ppm for the relative acoustic velocity and 10% for the total attenuation are routinely obtained with this interferometer.

Although some tests have been made at other frequencies, we report for the present work only results obtained using a longitudinal acoustic signal at 90 MHz (the first overtone of 30 MHz) propagating along the hexagonal $\hat{\mathbf{c}}$ axis. The orientation of the crystal in the magnetic field was controlled by a gearing system which allows all angles from 0 to 90°. The error in the orientation of the sample is believed to be mainly due to the misalignment of the plane of rotation, an error that we estimate to be much less than 5°. The sample temperature was monitored with two sensors; a carbon glass resistance for temperature measurements in the presence of a magnetic field and a diode sensor mounted directly on the sample for the zero-field measurements. The carbon glass resistance was calibrated on the diode temperature readings in zero field. Those sensors were controlled by a Lakeshore DRC-93C system.

It is easier to define transition points by calculating the derivative of the data. Such a treatment requires an enormous amount of data points to reduce noise. Magnetic field and temperature have been incremented by as little as 100 G and 1 mK, respectively. Each of the phase diagrams reported here are made in a single-day experiment, and generate as many as 10 000 data points.

Since $CsNiCl_3$ is an insulator, very special care is needed to avoid thermal gradients. To this end, the sample and temperature sensors were put inside a copper box as a thermal shield with the heater resistance outside the box. It is our experience that the use of the box can lower the temperature readings by a few tenths of a degree when heating is high ($T > 5$ K). Considering the scale of temperature of interest, this correction is quite important.

In order to construct a phase diagram, it is necessary to track anomalies on the quantity measured as a function of external parameters. The anomalies in the acoustic velocity are usually better defined and narrower than the ones in the attenuation. Consequently, the phase diagrams reported here were made using the acoustic velocity and the attenuation has been used as a confirmation. Except when we intended to test the presence of hysteresis, all the transition points were obtained with increasing temperature or magnetic field.

III. RESULTS

The anomalies in $\Delta v/v$ as a function of temperature at $H = 0$ and 2.5 T parallel to the $\hat{\mathbf{c}}$ axis are presented in Fig. 1. The arrows in this figure indicate where the transition points were chosen. They correspond, when it is possible, to where the derivative of $\Delta v/v$ is the largest. At $H = 0$, the small dip at T_{N_1} (L-P transition) and the large step at T_{N_2} (E-L) are shown. For $\mathbf{H} \parallel \hat{\mathbf{c}}$ and field values above the multicritical point, such as $H = 2.5$ T, only one large anomaly at T_c corresponding to the SF-P transition can be observed (see Ref. 7 for notation).

A different signature of the transitions is presented in Fig. 2 where data are plotted as a function of the magnetic field parallel to the $\hat{\mathbf{c}}$ axis for two fixed temperatures; 4.4 and 4.6 K. The lower field anomaly at $T = 4.4$ K corresponds to the transition line emerging from T_{N_2} at $H = 0$. The shape of the step in this figure is reversed from that of Fig. 1 since the L phase appears at higher T in the former and lower H in the latter. The other critical field observable at this temperature is the spin-flop field at $H \approx 2.1$ T (E-SF). At $T = 4.6$ K there are also two observable anomalies, corresponding to the transitions L-P at the lower-field dip and P-SF at the stronger step.

Since the magnetic and the elastic properties are linked, the choice of largest derivatives of $\Delta v/v$ to indicate the transition points is supported by the argument

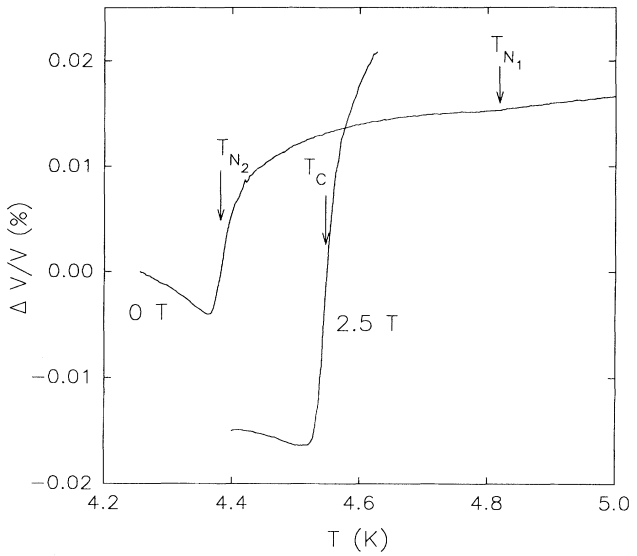

FIG. 1. Relative acoustic velocity as a function of T at $H = 0$ and 2.5 T parallel to the $\hat{\mathbf{c}}$ axis. Arrows indicate where the transition temperatures were chosen.

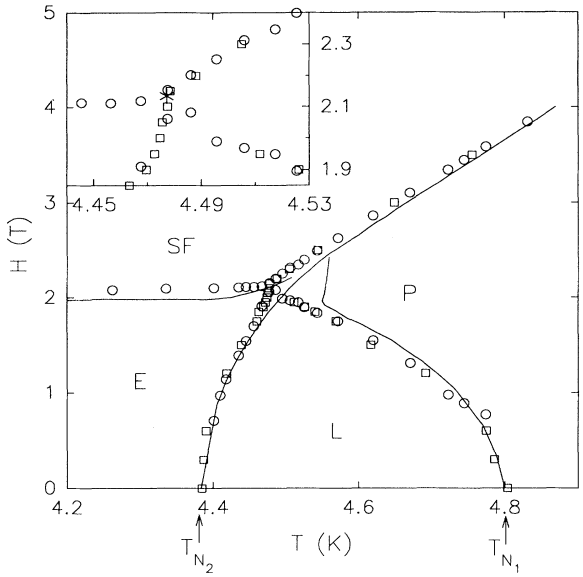

FIG. 3. Magnetic phase diagram as determined from acoustic velocity anomalies for $\mathbf{H} \parallel \hat{\mathbf{c}}$. The squares are critical temperatures obtained at constant field and the circles are critical fields obtained at constant temperature. The lines correspond to the case where $\mathbf{H}$ is directed 10° away from $\hat{\mathbf{c}}$ and are hand drawn through the data points. The inset shows the region near to the multicritical point. The estimated position of the multicritical point is indicated by the star.

that the magnetic properties experience the largest variation at a phase transition. Although this choice is somewhat arbitrary, slightly different indicators of a transition yield qualitatively the same phase diagram. A consistent determination is, however, desirable as we can, in most cases, make two independent estimates of a critical point by field sweeps or temperature sweeps. The relative amplitudes and widths of the anomalies give an estimate of the error in the critical-point values.

The phase diagram determined in this way with $\mathbf{H} \parallel \hat{\mathbf{c}}$ is presented in Fig. 3. It is clear from these results, which are the most detailed presented to date for this material, that the three critical lines do indeed merge with the spin-flop line at a common point.[7] This diagram is similar to those found in the literature,[5,6] except for the high-field SF-P line whose slope as a function of temperature is larger in the present work. This larger slope is explained by the absence of thermal gradient. Without the thermal shield there will be a positive error on the temperature readings proportional to $(T - 4.2\ \text{K})$. This error will give a smaller slope for the lines extending toward high temperatures like the SF-P line. The inset of Fig. 3 shows the region near the multicritical point. This point (the star) is found to be located at $T_M = 4.48$ K and $H_M = 2.13$ T. These values are similar to those reported by Poirier *et al.*[6] This figure also includes hand-sketched lines through the experimental critical points in the case where $\mathbf{H}$ is directed 10° away from $\hat{\mathbf{c}}$. The phase diagram is not changed very much for this field angle, the only significant difference is the up-turn of the L-P line near the multicritical point.

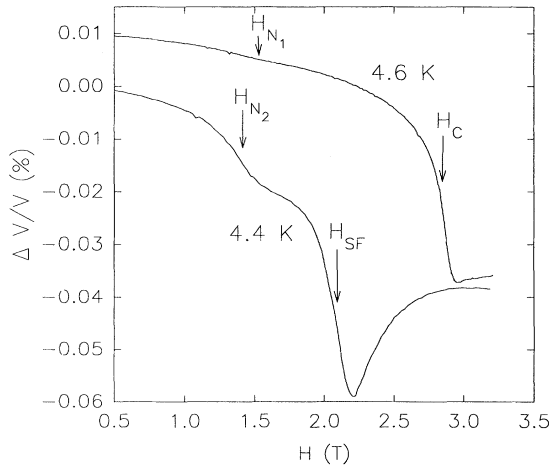

FIG. 2. Relative acoustic velocity as a function of H parallel to the $\hat{\mathbf{c}}$ axis at $T = 4.4$ and 4.6 K. The arrows indicate where the critical fields were chosen.

The phase diagram for $\mathbf{H} \perp \hat{\mathbf{c}}$ is shown in Fig. 4. At such a field orientation, the phase diagram is formed by three open phases; P, L, and E. The lines bounding these phases originate from T_{N_1} and T_{N_2} at zero field and move toward higher temperatures as the field is increased. At a sufficiently high field the two lines appear parallel. This phase diagram is also quite similar to the one obtained by Johnson *et al.*[5] except that the slopes are larger in the present work. Hand-drawn lines through the critical points with $\mathbf{H}$ directed 50° away from $\hat{\mathbf{c}}$ are also shown. These results, together with those of Fig. 3, demonstrate that the E-L line is relatively independent of field orientation. This is in contrast with the L-P transition line that is pushed significantly toward lower temperature.

Further details of the angular dependence of the phase diagram are presented in Figs. 5 and 6. Figure 5 contains

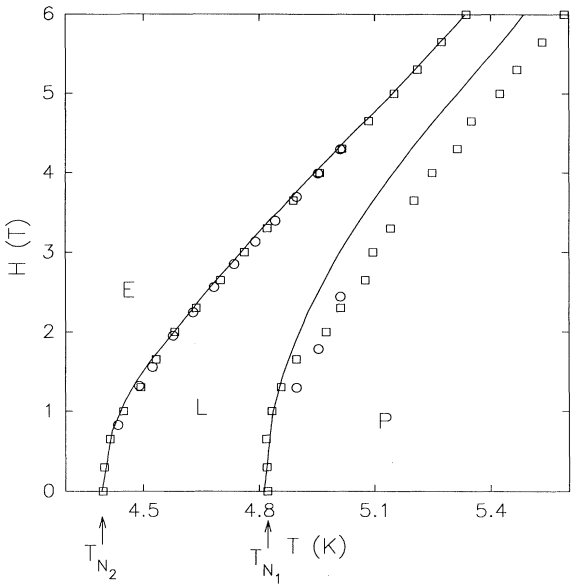

FIG. 4. Magnetic phase diagram as determined from sound-velocity anomalies for $\mathbf{H} \perp \hat{\mathbf{c}}$. The squares are critical temperatures obtained at constant field and the circles are critical fields obtained at constant temperature. The lines come from a hand sketch through the critical points with $\mathbf{H}$ 50° off $\hat{\mathbf{c}}$.

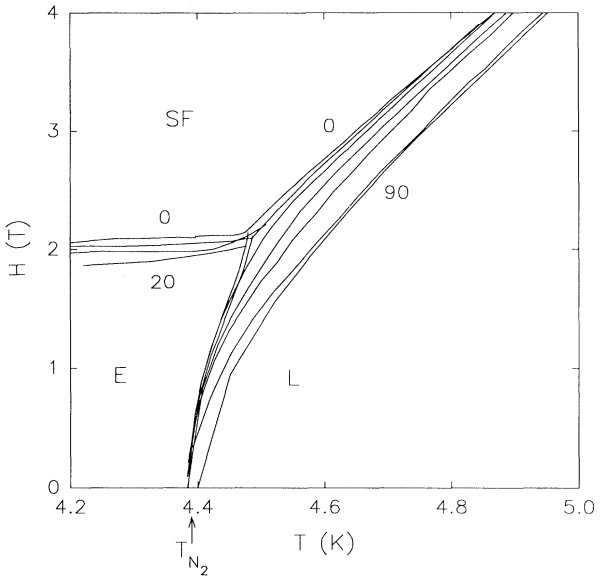

FIG. 5. Hand-sketched lines of the low-temperature transition lines otained from data with $\mathbf{H}$ at angles 0, 5, 10, 20, 30, 50, 390° off $\hat{\mathbf{c}}$. The labels indicates the angle of the nearest line.

only (for clarity) the lines originating from the E-L, E-SF, and SF-P transitions which occur at $\mathbf{H} \parallel \hat{\mathbf{c}}$. The other transition line, L-P, is presented in Fig. 6. These lines are hand-sketched through the data points and they are presented in this way to improve readability and give the general behavior only. The numerical label indicates the field orientation of the closest line. In Fig. 5, the successive field angles for the E-L and SF-P transition lines are 0, 5, 10, 20, 30, 50, and 90°. The line E-SF has been observed only up to 20°. At higher field angles, the difference between the E and SF phases tends to disappear and it is no longer possible to track the anomaly. One can also notice that the discontinuity at the junction between the E-L and SF-P lines seems to disappear for field angles larger than 5°.

The higher-temperature L-P transition line is presented in Fig. 6 for field angles 0, 5, 10, 20, 30, 50, and 90°. The 0 and 5° lines are superimposed. This transition line shows a large field orientation dependence. At the smaller field angles, behavior reminiscent of the multicritical point is seen. Within the experimental resolution, the junction between the L-P and L-$SF(E)$ lines has been observed up to a field angle of 20°.

As one can notice by looking at Figs. 5 and 6 there is a slight spread in T_{N_1} and T_{N_2} values from one experiment to another. The average T_{N_1} and T_{N_2} values found are, respectively, 4.80 and 4.388 K with standard deviations of 0.01 and 0.004 K. Of course, these errors do not include the absolute accuracy of the temperature sensors which is evaluated to 0.03 K. These values are comparable with the ones found in the literature.[4–6]

The discontinuity near the multicritical point on the L-P line at field angle of 10° seen in Fig. 3 has been found to be linked to another transition line that extends into the phase L. The anomalies in $\Delta v/v$ and in the acoustic attenuation, related to this transition, are presented in Fig. 7 for a field angle of 50° at $T = 4.63$ K. The anomaly in $\Delta v/v$ is quite small and corresponds to

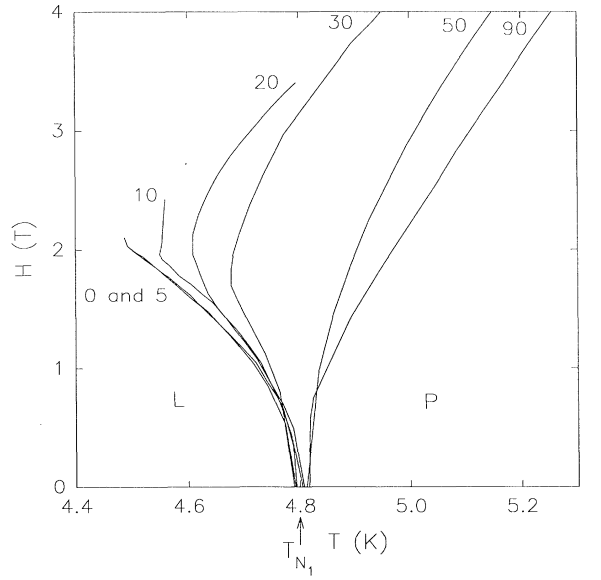

FIG. 6. Hand-sketched lines of the high-temperature transition lines obtained from data with $\mathbf{H}$ at an angle 0, 5, 10, 20, 30, 50, 90° off $\hat{\mathbf{c}}$. The labels indicates the angle of the nearest line.

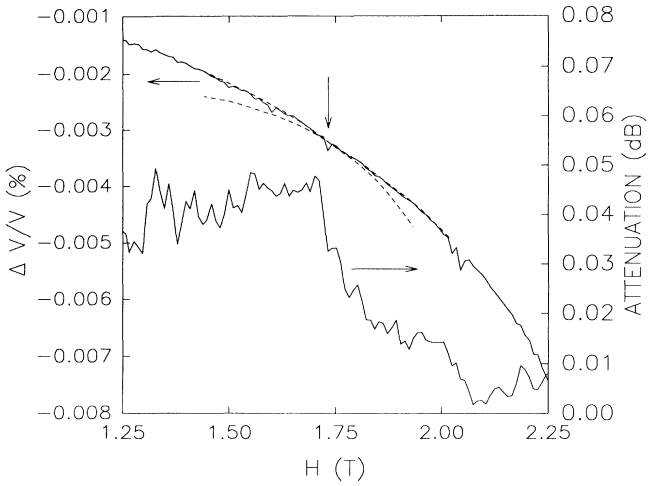

FIG. 7. Acoustic velocity and attenuation as a function of H, with **H** directed 50° from $\hat{\mathbf{c}}$ at $T = 4.63$ K. Vertical arrow indicates estimated transition point and broken lines show the change in curvature on $\Delta v/v$ at the transition.

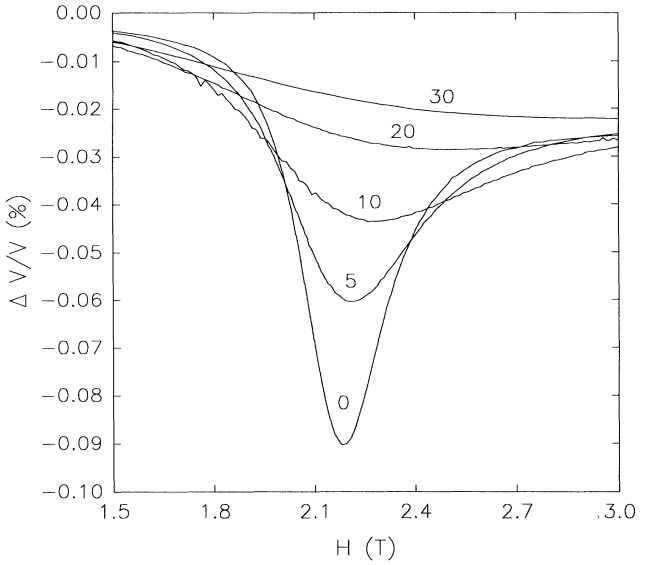

FIG. 8. Relative acoustic velocity at the spin-flop anomaly as a function of magnetic field for **H** at angles 0, 5, 10, 20, and 30° from $\hat{\mathbf{c}}$ taken at $T = 4.2$ K.

a slight change in curvature, but in the attenuation the anomaly looks like a step and it is much easier to define. Here is a good example of the use of the acoustic attenuation which seems to be much more sensitive to this anomaly. Since this anomaly is fairly weak, we first thought it was an artifact, but every attempt to reduce the noise and improve the signal stability has resulted in an improvement of the transition visibility. In order to avoid confusion, this transition line has not been plotted on the phase diagrams, but it has been seen with the sample oriented at 10, 20, 30, and 50°. It has been observed only in field sweeps and its critical field seems to be approximately constant. A possible explanation is given in Sec. IV.

Figure 8 shows the angular dependence of the spin-flop anomaly E-SF, which disappears at larger angles. In this figure, magnetic-field sweeps made at $T = 4.2$ K are presented for field angles 0, 5, 10, 20, and 50°. At $\mathbf{H} \parallel \hat{\mathbf{c}}$ the anomaly has the shape of a narrow and deep minimum, a shape that is qualitively different from the step of the other anomalies (see Figs. 1 and 2). The depth of the anomaly is reduced as the field angle is increased, up to 20° after which there is no longer a minimum. The position of the minimum is nearly field angle independent (see Sec. IV). For $\mathbf{H} \parallel \hat{\mathbf{c}}$ the change in spin orientation involves a 90° flop but is a gradual reorientation for other field directions (see Sec. IV). As a result, the anomaly evolves from a narrow minimum at $\mathbf{H} \parallel \hat{\mathbf{c}}$ to a much shallower dip at 30°.

As a function of the temperature, the evolution of the spin-flop anomaly is also of interest. Figure 9 displays different curves for $\mathbf{H} \parallel \hat{\mathbf{c}}$ and fixed temperatures of 2, 2.5, 3, 3.5, and 4 K. The amplitude of the anomaly is diminished and the position of the minimum is displaced toward higher field when the temperature is increased. The temperature dependence of the amplitude also seems to be nonlinear. Experiments have also been conducted, for each of these temperatures, in increasing and decreasing fields to check for any hysteresis at this transition. We have found that if there is hysteresis, it is much smaller than our experimental resolution—less than 100 G. A possible explanation, explored in the next section, is that this phase transition may not be first order. The absence of hysteresis in this transition has also been observed in other similar quasi-one-dimensional magnetic systems[12] displaying a spin-flop transition such as $CsMnI_3$ and $CsNiBr_3$. One could argue from the strong angular de-

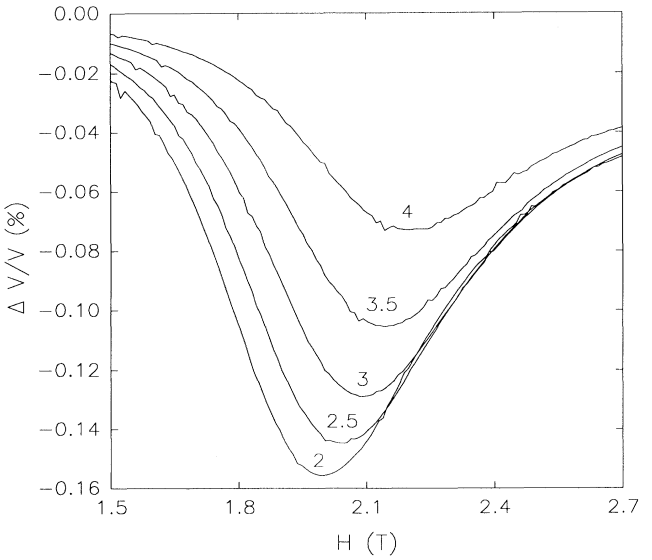

FIG. 9. Relative acoustic velocity at the spin-flop anomaly as a function of magnetic field at $T = 2$, 2.5, 3, 3.5, and 4 K.

pendence of this transition that it would be first order only when the field will be oriented exactly along the $\hat{\mathbf{c}}$ axis. Such an alignment, even with a double axis system, is very difficult to achieve since the defaults in the crystal induce some nonparallelism among the chains.

The absence of hysteresis has also been verified for the other phase transitions as a function of either the temperature or the magnetic field. This is expected since these are believed to be continuous.

IV. THEORY

There are two similar mean-field models which have been used to develop a Landau-type free energy to explain the phase diagrams of $CsNiCl_3$ and related materials.[13] One formulation is phenomenological and based only on symmetry arguments, having a relatively large number of unknown coefficients of the independently invariant terms involved.[7] Apart from gaining a qualitative understanding of the nature of the magnetically ordered phases, a fitting of these numerous coefficients to experimental data allows for the possibility of spectacularly good agreement with measured phase boundary lines. The other approach generates an equivalent Landau-type free energy using a molecular-field treatment of the Hamiltonian (1); the only parameters involved are thus $J_{\|}$, $J_{\perp}$, and D.[13] Provided that D is reasonably small, this approach yields a qualitatively similar phase diagram. A useful characterization of the magnetic phases is through the spin density

$$\mathbf{s}(\mathbf{r}) = \mathbf{m} + \mathbf{S}e^{i\mathbf{Q}\cdot\mathbf{r}} + \mathbf{S}^{*}e^{-i\mathbf{Q}\cdot\mathbf{r}}, \quad (4)$$

where $\mathbf{m}$ is the uniform component induced by the field, $\mathbf{Q}$ is the wave vector, and the complex polarization vector can be written as $\mathbf{S} = \mathbf{S}_a + i\mathbf{S}_b$. (In order to distinguish the many different types of ordered phases we revert to the number labeling as described in Ref. 14.) In the paramagnetic phase 1 (P) $S = 0$, and the ordered phases have the following nonzero components: phase 2 (L), S_a^z; phase 3 (E), S_a^z and S_b^x; and phase 4 (SF), S_a^y and S_b^x. The phase diagram of Ref. 7 was generated with the reasonable assumption that $\mathbf{m} \parallel \mathbf{H}$. We consider here the effects of relaxing this assumption as well as the magnetic phases stabilized when the field is not along the $\hat{\mathbf{c}}$ axis. Both the phenomenological and molecular-field models are analyzed here.

In connection with the absence of hysteresis at the 1-4 spin-flop phase boundary for the case of $\mathbf{H} \parallel \mathbf{c}$, the result of relaxing the constraint $\mathbf{m} \parallel \mathbf{H}$ in the phenomenological model was surprising. Using the same parameters as in Ref. 7, an intermediate elliptical phase 8, with nonzero S_a^x, S_a^z, and S_b^y was stabilized so that the first-order 1-4 transition now becomes two continuous transitions, 3-8 and 8-4, with increasing field. (A similar result was reported in Ref. 14 [Fig. 1(d)] to be a consequence of including higher-order anisotropy effects.) The range of field over which phase 8 is stable was found to be very small, as shown in Fig. 10, as was the component of $\mathbf{m}$ perpendicular to $\mathbf{H}$. This feature is dependent on the parameter values but the vanishing width of stability of this phase with increasing temperature is a universal property. The 3-8 and 8-4 boundary lines merge at the multicritical point, which now represents the confluence of *five* phases.[15] Notably, this new phase 8 does not occur in the molecular-field treatment of the Hamiltonian (1) or in an exact calculation at $T = 0$ using realistic (or otherwise) parameter values. In addition, no evidence for such a phase has been observed in Monte Carlo simulations of the Hamiltonian (1).[16] It thus appears that other types of interactions, possibly biquadratic exchange,[17] would be required to stabilize this state in the microscopic model. It remains, however, an interesting possibility that these results are relevant to the absence of observed hysteresis.

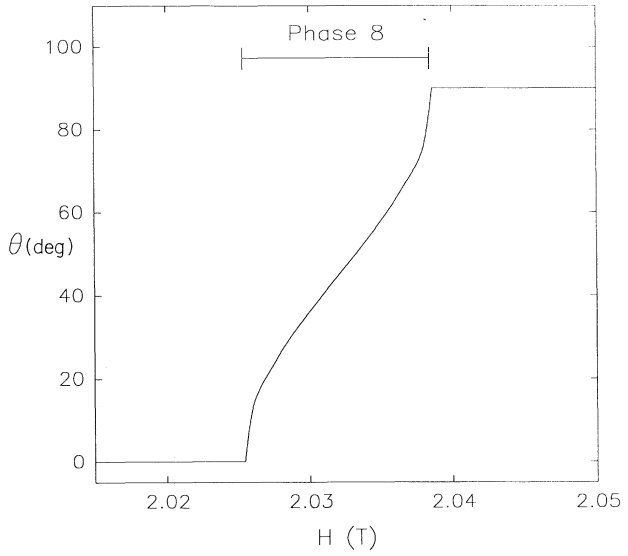

FIG. 10. Narrow range of stability of the intermediate phase 8 from the phenomenological model using parameters from Ref. 7. Shown is the field dependence of the angle $\theta = \tan^{-1}(S_a^y/S_a^z)$, where $\theta = 0$ for phase 3 and $\theta = \pi/2$ for phase 4.

A perhaps more realistic explanation for the absence of observed hysteresis may be found in the theoretical and experimental results for spin-waves near the 3-4 transition at low T.[18] One of the modes is found to be zero, and other modes nearly so for $J_{\perp} \ll J_{\|}$, at the critical field in a manner similar to the usual soft-mode phenomena at a continuous transition. This means that such a system may easily generate the excitations necessary to overcome the energy barrier between the two phases at the transition and make any hysteresis effects negligible. There is, however, a small discrepancy between the work of Ref. 18 and our own results concerning the evolution of phases with increasing field at $T = 0$.[16] The symmetry of the phase $3A$ which appears at the spin-flop field, which was determined numerically in Ref. 16, is different from the one $3B$, assumed in Ref. 18. (Two linear phases of different symmetry, $2A$ and $2B$, also exist and are separated in the phase diagram by a first-order transition.[13] The additional anomaly observed in the L phase as discussed in the previous section, and shown in

Fig. 7, may be related to this transition.) Fortunately, this difference is negligible for the case $J_\perp \ll J_\parallel$ so that the principal conclusions of Ref. 18 are correct for systems like $CsNiCl_3$. We performed a calculation in order to estimate the barrier ΔE between phases 3 and 4 at $T = 0$ by examining the energy as a function of the angle $\theta = \tan^{-1}(S_a^y/S_a^z)$, where $\theta = 0$ for phase 3 and $\theta = \pi/2$ for phase 4. Using the parameters $J_\parallel = -1$ and $D = 0.01$, the results $\Delta E = 0.5$ and $\Delta E = 0.01$ for $J_\perp = 1$ and 0.02, respectively, indicate that a negligible energy barrier can occur for this transition if the exchange interactions are quasi-one-dimensional.

Both models gave essentially the same results for the structure of the phase diagram in the cases where the applied field is not parallel to the $\hat{\mathbf{c}}$ axis. The principal effect of having an in-plane component to the field is that the spin-flop transition is eliminated and the region formerly occupied by phases 3 and 4 now becomes one state only, elliptical (E) phase 8. For small in-plane field components, however, there remains a rapid variation of the spin structure as characterized by the angle θ with increasing field shown in Fig. 11. It is thus not unreasonable to expect the possibility of anomalous behavior in some thermodynamic quantities at, for example, the field value where the slope exhibits a point of inflection. Note that this signature is relatively independent of field orientation. These results are consistent with the experimental data shown in Fig. 8. Note that these data show a reduction in the anomaly as the temperature is increased. It is a prediction of the theory that the latent heat associated with the SF transition (for $\mathbf{H} \parallel \hat{\mathbf{c}}$) tends to zero at the multicritical point, a result which is supported by the data of Fig. 9. In addition to the modification of the elliptical state, the linear (L) state now has the symmetry of phase 9 of Ref. 14, with nonzero spin components S_a^x and S_a^z. Illustrative results for the case where $\mathbf{H}$ is directed 10° from $\hat{\mathbf{c}}$ are presented in Fig. 12, which are based on the phenomenological model using the same parameters as in Ref. 7. A universal feature of these models is that the linear phase persists at high-field values, but occupying a smaller region of the phase diagram. This is in contrast with the observation (see Fig. 3) of only one phase boundary line at high-field values in the experimental results for $\mathbf{H}$ 10° off $\hat{\mathbf{c}}$. This discrepancy may be a result of insufficient experimental resolution or of critical-fluctuation effects neglected in the mean-field models. The general trends seen experimentally in Figs. 5 and 6 with increasing angle are, however, reproduced by both models.

The mean-field models may also be used to predict the anomalous behavior in the elastic constants (and thus the sound velocity).[19] To lowest order in the magnetoelastic coupling, phase transitions induce simple step discontinuities, unlike what has been observed in $CsNiCl_3$. We note, however, that higher-order couplings can lead to the possibility of more complicated temperature and field dependences in the region of a transition, as seen experimentally. Critical-fluctuation effects are also likely to be important in determining the quantitative behavior. Based on such considerations, the minima (and not steplike behavior) shown in Fig. 8 at the SF transition are not surprising.

Finally we consider the results of scaling and renormalization-group theory concerning the behavior of the critical lines near the multicritical point.[20] It is predicted that all three lines are governed by the same crossover exponent $\phi \simeq 1$ and that each approaches the spin-flop line tangentially. It is evident from the inset on Fig. 3 that although the upper curve is consistent with this behavior, it is not clear that the other two lines ex-

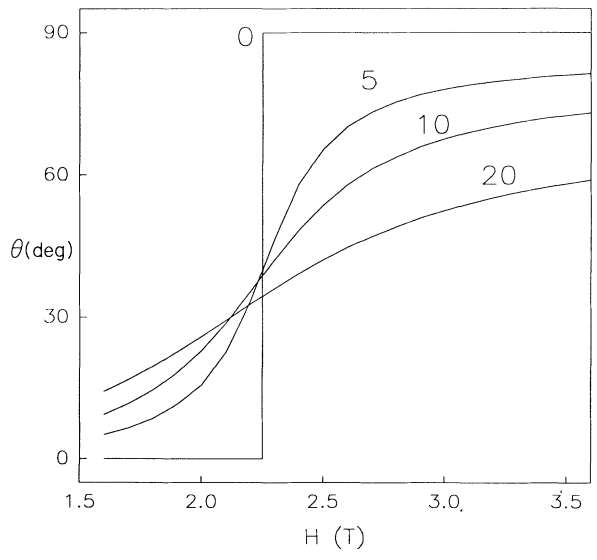

FIG. 11. Field dependence of the angle $\theta = \tan^{-1}(S_a^y/S_a^z)$ from phenomenological model using parameters from Ref. 7 for field orientations $\mathbf{H}$ 0, 5, 10, and 20° away from $\hat{\mathbf{c}}$.

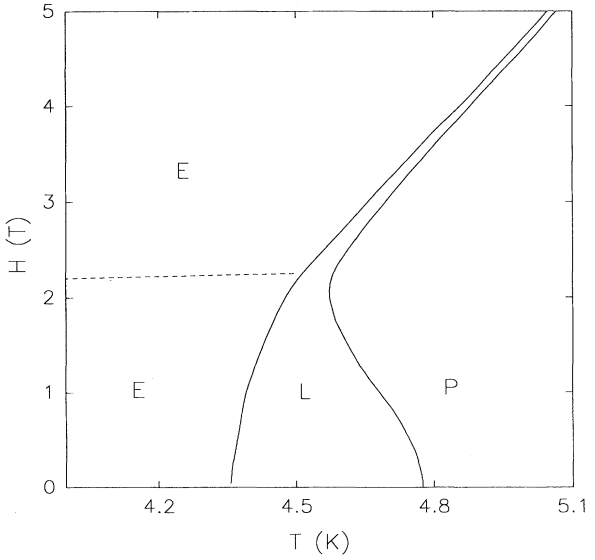

FIG. 12. Mean-field phase diagram for $\mathbf{H}$ 10° from $\hat{\mathbf{c}}$ obtained from the phenomenological model. Broken line indicates point of inflection in $\theta(H)$ as shown in Fig. 11.

hibit this tendency. It is likely that the true structure is observable only in a region much closer to the multicritical point than is accessible by the present techniques. Following the method described in Ref. 6, a numerical fit of the data was attempted in order to estimate the exponent ϕ, but with unsatisfactory results.

V. CONCLUSIONS

The phase diagrams for $\mathbf{H} \parallel \hat{\mathbf{c}}$ and $\mathbf{H} \perp \hat{\mathbf{c}}$ have been reproduced successfully and with a greater precision than previous results. Some quantitative differences have been attributed to the presence of a thermal shield that helped to remove temperature gradients inside the sample. As a function of the angle between the magnetic field and the $\hat{\mathbf{c}}$ axis we have been able to observe the displacement of the transition lines in the phase diagrams. With this knowledge, we are able to provide a clear picture of how the structure of the phase diagram is transformed from $\mathbf{H} \parallel \hat{\mathbf{c}}$ to $\mathbf{H} \perp \hat{\mathbf{c}}$. The general behavior of the phase diagram is compatible with the mean-field models of Plumer *et al.*[13]

A new transition line has been detected for some intermediate field orientations, in the linear phase L. This phase transition may be related to the one that is labeled $2A$-$2B$ (for $\mathbf{H} \parallel \hat{\mathbf{c}}$) in Ref. 13. However, if it is the same transition, it should also be present in phase E ($3A$-$3B$) and for $\mathbf{H} \parallel \hat{\mathbf{c}}$. These two predictions have not been verified experimentally.

The behavior of the spin-flop anomaly on $\Delta v/v$ as a function of the orientation of the sample in the magnetic field and as a function of the temperature at which the field was swept, was recorded. We have found that the amplitude of the anomaly is reduced by increasing the angle between the field and the $\hat{\mathbf{c}}$ axis and by increasing the temperature. No hysteresis has been observed in this anomaly. These features are accounted for with the mean-field models. A true spin-flop transition, with a strong anomaly, can occur only for a configuration $\mathbf{H} \parallel \hat{\mathbf{c}}$. The absence of observable hysteresis is believed to be a result of the quasi-one-dimensional nature of the exchange interactions but may also be a consequence of the existence of an intermediate phase.

The presence of a new phase transition in the linear phase L should be confirmed along with its absence from phase E. The behavior of the width of the spin-flop anomaly as function of the temperature requires better understanding since it is a key element to whether or not this anomaly is formed by one first-order or two second-order transitions. If the latter case is observed, additional (and yet unkown) interactions to the simple and widely assumed Hamiltonian (1) will be required for a better understanding.

ACKNOWLEDGMENTS

Financial support from the Centre de Recherche en Physique du Solide, the Natural Sciences and Engineering Research Council of Canada, and le Fonds Formation de Chercheurs et l'Aide à la Recherche du Gouvernement du Québec has been essential for this work. We also thank M. Castonguay for technical assistance, W. J. L. Buyers for the high-quality crystal, and A. Chubukov for enlightening correspondence.

[1] F. D. M. Haldane, Phys. Lett. **93A**, 464 (1983); Phys. Rev Lett. **50**, 1153 (1983).
[2] M. L. Plumer and A. Caillé, Phys. Rev. Lett. **68**, 1042 (1992).
[3] W. J. L. Buyers, R. M. Morra, R. L. Armstrong, M. J. Hogan, P. Gerlach, and K. Hirakawa, Phys. Rev. Lett. **56**, 371 (1986); R. M. Morra, W. J. Buyers, R. L. Armstrong, and K. Hirakawa, Phys. Rev. B **38**, 543 (1988).
[4] R. H. Clark and W. G. Moulton, Phys. Rev. **35**, 788 (1972).
[5] P. B. Johnson, J. A. Rayne, and S. A. Fridberg, J. Appl. Phys. **50**, 1853 (1979).
[6] M. Poirier, A. Caillé, and M. L. Plumer, Phys. Rev. B **41**, 4869 (1990).
[7] M. L. Plumer, K. Hood, and A. Caillé, Phys. Rev. Lett. **60**, 45 (1988).
[8] Y. Trudeau, M. Poirier, and A. Caillé, Phys. Rev. B **46**, 169 (1992).
[9] G. Gorodetshy and I. Lachterman, Rev. Sci. Instrum. **52**, 1387 (1981).
[10] J. A. Rayne, J. G. Collins, and G. K. White, J. Appl. Phys. **52**, 1977 (1980).
[11] J. A. Rayne, J. G. Collins, and G. K. White, J. Appl. Phys. **55**, 2404 (1984).
[12] H. A. Katori, T. Goto, and Y. Ajiro, J. Phys. Soc. Jpn. **62**, 743 (1993).
[13] M. L. Plumer and A. Caillé, J. Appl. Phys. **70**, 5961 (1991).
[14] M. L. Plumer, A. Caillé, and K. Hood, Phys. Rev. B **39**, 4489 (1989).
[15] The Gibbs phase rule for an m-component fluid states that the number n of coexisting phases is governed by $n \leq m + 2$. Magnetic systems described by a three-component spin vector may thus exhibit this type of multicritical point; J. L. Lebowitz, J. Stat. Phys. **15** 463 (1977).
[16] A. Mailhot, M. L. Plumer, and A. Caillé, J. Appl. Phys. **67**, 5418 (1990); A. Mailhot, M. L. Plumer, and A. Caillé, Phys. Rev. B (to be published).
[17] A. V. Chubukov and D. I. Golosov, J. Phys.: Condens. Matter **3**, 69 (1991).
[18] I. A. Zaliznyak, L. A. Prozorova, and A. V. Chubukov, J. Phys.: Condens. Matter **1**, 4743 (1989); I. A. Zaliznyak, L. A. Prozorova, and S. V. Petrov, Zh. Eksp. Teor. Fiz. **97**, 359 (1990) [Sov. Phys. JETP **70**, 203 (1990)].
[19] M. L. Plumer and A. Caillé, Phys. Rev. B **37**, 7712 (1988).
[20] H. Kawamura, A. Caillé, and M. L. Plumer, Phys. Rev. B **41**, 4416 (1990).